

# A framework of ground truth event locations across Iran from a two tiered multi-event relocation approach

T1.2-P2

Ezgi Karasözen,<sup>1</sup> Eric A. Bergman<sup>2</sup> and Edwin Nissen<sup>3</sup>

1. Geophysics, Colorado School of Mines 2. Global Seismological Services, Golden, CO  
3. School of Earth and Ocean Sciences, University of Victoria



ekarasoz@mines.edu



## 2 Event Calibration

**mloc** is a multiple event relocation technique [Bergman and Solomon, 1990, GJR; Walker et al., 2011, JGI], based on Jordan and Sverdrup [1981, SSA]'s hypocentral decomposition method.

Like many other multi-event location methods, **mloc** estimates improved relative locations of clustered events by minimizing path-correlated errors in travel-times.

Unlike other methods, **mloc** has been specialized to determine **calibrated locations** - latitude, longitude, **depth** and **origin time** - when appropriate data sets are available.

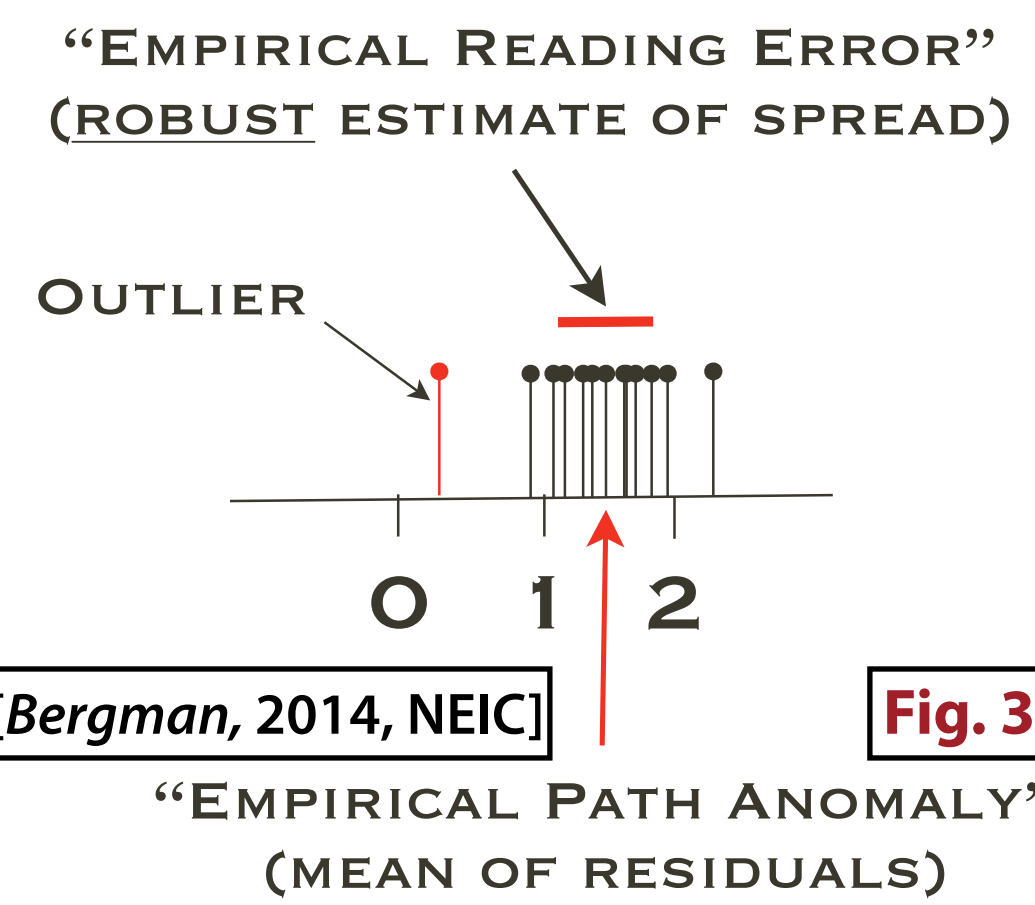
**mloc** separates the inversion problem into two steps, each using different datasets:

(1) Relocation of the cluster vectors, in which all available data are used, giving **relative locations**.

(2) Relocation of the hypocentroid, in which direct arrival phases  $Pg$  and  $Sg$  (at distances  $<1^\circ$ ) are preferred, giving **absolute locations**, and hence reduces the bias coming from the unknown earth structure.

The location uncertainty is fully quantified and calibrated and is estimated from the actual data.

**mloc** departs from standard practice in dealing with outlier arrival time readings by emphasizing consistency between repeated readings (of a given phase from different events in a cluster to the same station) rather than the size of residual against some reference travel time model (Fig. 3).



## 1 Introduction

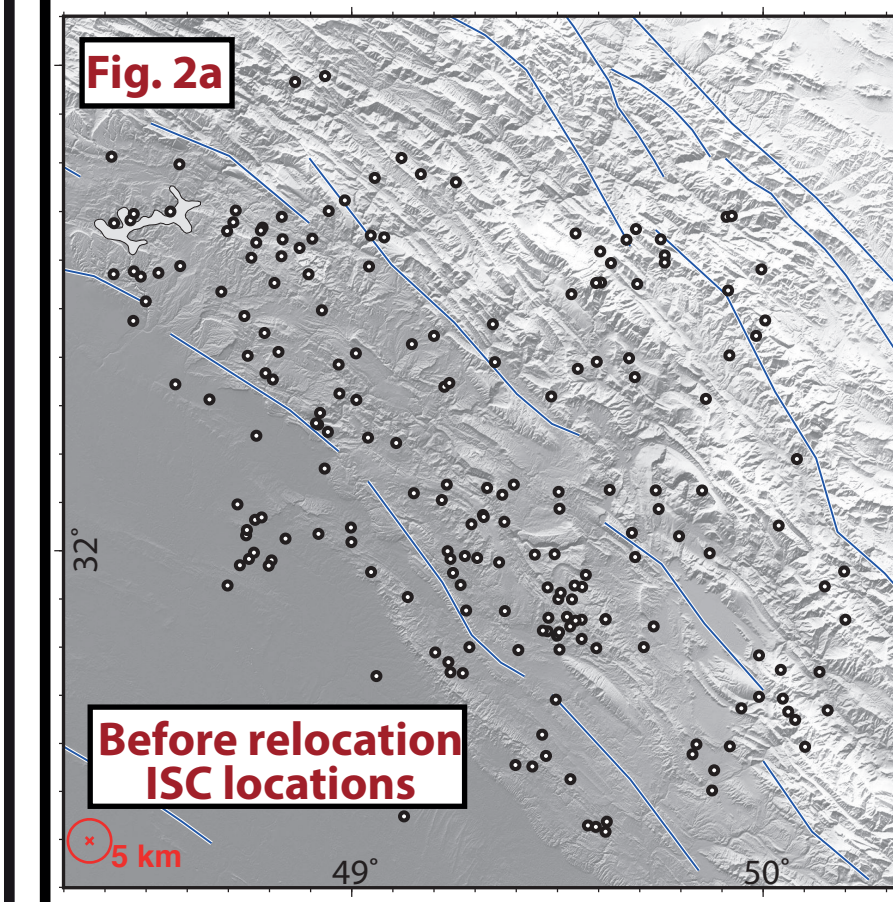
Uncertainties in standardized earthquake locations, which run into tens-of kilometers in many regions of the world, are a serious limitation to seismotectonic studies and nuclear treaty monitoring.

We have developed a new two-tiered multiple-event relocation approach that seeks to improve upon these catalog locations, and have applied it to Iran (Fig. 1a), a country with abundant seismicity ( $> 40,000$  ISC Bulletin events since 1960), a recent surge in station coverage, but with known shortcomings in location accuracy.

Our purpose is to generate a comprehensive catalog of calibrated, relocated earthquake hypocenters for the entire Iran region, by:

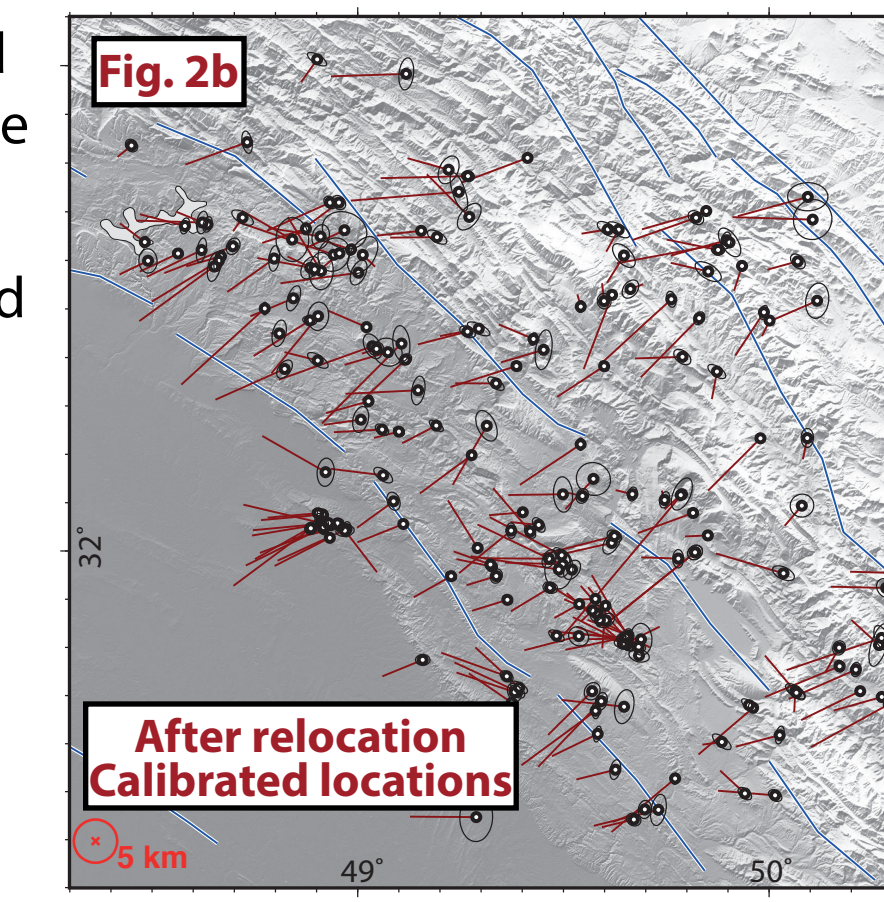
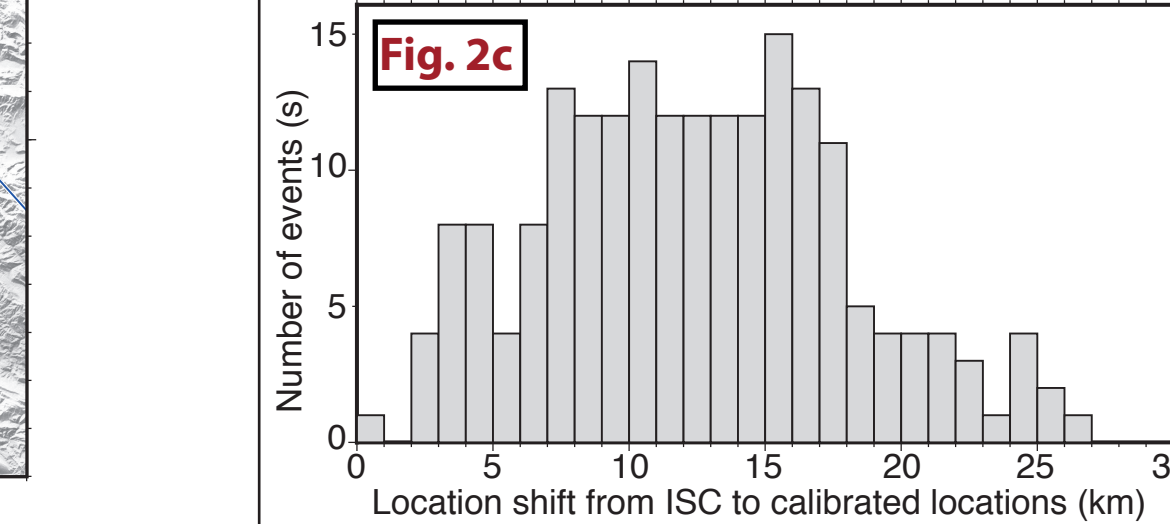
(1) developing **calibrated** earthquake clusters using near source data, aftershock deployments, and InSAR studies using **mloc** (panels 1 - 5). These clusters will not only include calibrated epicenters, but also hypocenters whose depth and origin time are well-constrained with rigorously-assessed errors.

(2) incorporating this backbone of trusted hypocenters into **Bayesloc**, thereby extending the analysis to the whole of Iran and the full back-catalogue of instrumental seismicity (panel 6).



From Fig. 2a to Fig. 2b: After the relocation, scattered seismicity in the Shushtar cluster collapses into discrete clusters and trends.

Confidence ellipses show with 90% confidence bound for each absolute location, all less than 5 km.



## 3 Depth and origin-time calibration

Depth trades off with origin time: Distant stations. For this reason, depth is usually kept fixed in most multiple event relocation techniques.

For locally-recorded events, direct phase arrivals ( $Pg$  and  $Sg$ ) provide strong constraints on the focal depth.

We start by selecting "control events" which have good  $Pg$  and  $Sg$  readings, good azimuthal coverage, and depth control from close-in stations.

These control events are relocated separately in order to first constrain the focal depths and second to refine the local crustal velocity model.

Next we incorporate  $Pn$  and  $Sn$  arrival times for the same control events, thereby determining the crustal thickness and upper mantle velocity.

After establishing the control event focal depths and velocity model, non-control events (with few or no  $Pg$  readings) can be added to the cluster.

The origin time for a non-control event will be driven by the fit of its  $Pn$  readings (steep take-off angles) to those of the control events, for an assumed focal depth.

So, what happens if the assumed depth for the non-control event is wrong?

If the assumed depth is greater than the true depth, its origin time must be later to fit the  $Pn$  arrivals with shorter ray-paths, leading to a negative  $Pg$  residual.

$Pg$  arrivals at regional distances have no dependence on depth (ray-path lengths stay the same) but are affected by changes in origin time.

Figure 4: A new routine to calibrate depth and origin time. The diagram shows ray paths from a source to stations at different depths and distances, illustrating how depth and origin time trade off.

Figure 5: Direct Calibration. The diagram shows the process of determining cluster vectors and relocating the hypocentroid using near-distance data and appropriate crustal models.

Figure 6: Residuals for crustal phases, average over (0-1.0). The plot shows residuals for  $Pg$  (red x) and  $Sg$  (red circles) versus distance (degree). The average residuals are -0.0 (solid red line) and -0.0 (dashed red line).

Figure 7: Indirect Calibration. The diagram shows the process of determining cluster vectors and relocating the hypocentroid using an indirect calibration method.

Figure 8: Station coverage for the Murmuri cluster. The map shows the distribution of seismic stations and the resulting calibrated locations.

Figure 9: From clusters to regional catalogs. The diagram shows the process of extending the relocation analysis to a larger region.

## 4 Direct Calibration

In **direct calibration** mode, **mloc** uses direct crustal phases ( $Pg$  and  $Sg$ ) recorded at shorter epicentral distances ( $<1^\circ$ ) and well-enough distributed to allow the hypocentroid to be located using only these data (Fig. 5).

By keeping ray path lengths short, the accumulated traveltime error from unknown velocity structure and the possible location error are minimized.

The Dorud cluster (Fig. 6) was calibrated by using data up to 100 km for the hypocentroid (Fig. 6a and 6b). All the available data were used for the cluster vector calculation.

Calibration level for the entire cluster is 1.5 km, with 104 events having 1 - 3 km of location error (Fig. 6c).

Figure 6a: Map showing ray paths used in direct calibration of the hypocentroid in the Dorud cluster. Triangles denote seismic stations and black, open circles represent earthquakes. Red circles show radii of 100 km and 200 km about the hypocentroid.

Figure 6b: Residuals for crustal phases, average over (0-1.0). The plot shows residuals for  $Pg$  (red x) and  $Sg$  (red circles) versus distance (degree). The average residuals are -0.0 (solid red line) and -0.0 (dashed red line).

Figure 6c: Final absolute locations (unbiased). The map shows the calibrated locations for the Dorud cluster with confidence ellipses.

Figure 7a: Map showing calibrated clusters in the Zagros mountains of south-western Iran. These are one of the best rapidly-deforming and seismically-active fold-and-thrust belts on Earth, with abundant earthquakes of up to Mw 6.7.

Folding of sedimentary rocks is expressed at the surface by series of anticlines and synclines which dominate the range physiography. Mapped surface faulting with earthquakes is extremely rare, with most seismicity occurring on blind reverse faults buried beneath or within a thick sedimentary cover. Therefore, we need accurate earthquake locations to characterize active faulting at depth.

We have calibrated ~2000 events with errors less than 5 km, from 1956 to 2017. According to the depth analysis (panel 3), available from 40% of these events, average hypocenter depth is 12 km, with a range of 3 - 26 km. The error in hypocenter depth calculation is 2 - 4 km (Fig. 1b).

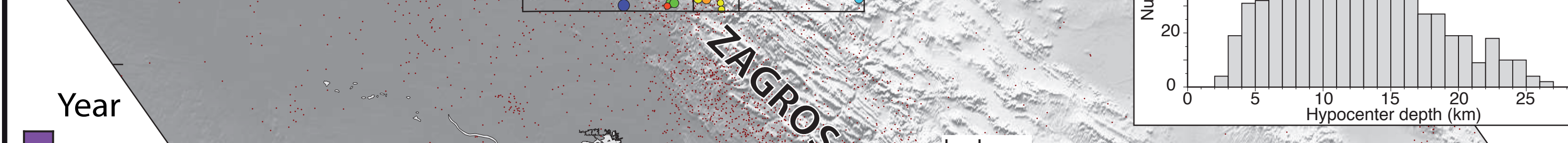


Figure 1b: Histogram showing the number of events versus hypocenter depth (km). The distribution is centered around 10-15 km.

Figure 1c: Map showing calibrated locations for the Murmuri cluster. The map shows the distribution of seismic stations and the resulting calibrated locations.

Figure 1d: Station coverage for the Murmuri cluster. The map shows the distribution of seismic stations and the resulting calibrated locations.

Figure 1e: Final absolute locations (unbiased). The map shows the calibrated locations for the Murmuri cluster with confidence ellipses.

Figure 1f: Final absolute locations (unbiased). The map shows the calibrated locations for the Murmuri cluster with confidence ellipses.

Figure 1g: Final absolute locations (unbiased). The map shows the calibrated locations for the Murmuri cluster with confidence ellipses.

This work is supported by AFRL Contract FA9453-15-C-0066 and NSF Grant EAR 1523815.phys. J. Int., 187, 1577-1603.

## 5 Indirect Calibration

In regions where near-source data are rare we can obtain calibrated locations using an **indirect calibration** (Fig. 7). This can be achieved if the location of one or more of the cluster events is known accurately from independent information, i.e. (1) previously published epicenters from local aftershock deployments, (2) recent magnitude 5-6 earthquakes that have been imaged with InSAR, (3) field mapping, (4) ground truth events, and (5) man-made explosions.

Locations are determined by shifting the entire cluster in space and time to match to the known location of the ground truth event(s).

The Murmuri cluster (Fig. 8a) had an azimuthal gap in near-source arrival time data of  $\sim 180^\circ$  to the SW. We first located the cluster vectors with teleseismic arrivals. Then, we calibrated the entire cluster using InSAR-derived fault planes.

Uncertainties in the positions of the model fault planes is an additional source of error, and is likely to be  $\sim 10$  km (Fig. 8b).

Figure 7a: Map showing calibrated clusters in the Zagros mountains of south-western Iran. These are one of the best rapidly-deforming and seismically-active fold-and-thrust belts on Earth, with abundant earthquakes of up to Mw 6.7.

Folding of sedimentary rocks is expressed at the surface by series of anticlines and synclines which dominate the range physiography. Mapped surface faulting with earthquakes is extremely rare, with most seismicity occurring on blind reverse faults buried beneath or within a thick sedimentary cover. Therefore, we need accurate earthquake locations to characterize active faulting at depth.

We have calibrated ~2000 events with errors less than 5 km, from 1956 to 2017. According to the depth analysis (panel 3), available from 40% of these events, average hypocenter depth is 12 km, with a range of 3 - 26 km. The error in hypocenter depth calculation is 2 - 4 km (Fig. 1b).

Figure 8a: Station coverage for the Murmuri cluster. Note the  $\sim 180^\circ$  azimuthal gap to the southwest and lack of near-source data at distances  $<100$  km.

Figure 8b: Final absolute locations (unbiased). The map shows the calibrated locations for the Murmuri cluster with confidence ellipses.

Figure 8c: Final absolute locations (unbiased). The map shows the calibrated locations for the Murmuri cluster with confidence ellipses.

Figure 8d: Final absolute locations (unbiased). The map shows the calibrated locations for the Murmuri cluster with confidence ellipses.

Figure 8e: Final absolute locations (unbiased). The map shows the calibrated locations for the Murmuri cluster with confidence ellipses.

Figure 8f: Final absolute locations (unbiased). The map shows the calibrated locations for the Murmuri cluster with confidence ellipses.

Figure 8g: Final absolute locations (unbiased). The map shows the calibrated locations for the Murmuri cluster with confidence ellipses.

Figure 8h: Final absolute locations (unbiased). The map shows the calibrated locations for the Murmuri cluster with confidence ellipses.

Figure 8i: Final absolute locations (unbiased). The map shows the calibrated locations for the Murmuri cluster with confidence ellipses.

Figure 8j: Final absolute locations (unbiased). The map shows the calibrated locations for the Murmuri cluster with confidence ellipses.

Figure 8k: Final absolute locations (unbiased). The map shows the calibrated locations for the Murmuri cluster with confidence ellipses.

Figure 8l: Final absolute locations (unbiased). The map shows the calibrated locations for the Murmuri cluster with confidence ellipses.

Figure 8m: Final absolute locations (unbiased). The map shows the calibrated locations for the Murmuri cluster with confidence ellipses.

Figure 8n: Final absolute locations (unbiased). The map shows the calibrated locations for the Murmuri cluster with confidence ellipses.

Figure 8o: Final absolute locations (unbiased). The map shows the calibrated locations for the Murmuri cluster with confidence ellipses.

Figure 8p: Final absolute locations (unbiased). The map shows the calibrated locations for the Murmuri cluster with confidence ellipses.

Figure 8q: Final absolute locations (unbiased). The map shows the calibrated locations for the Murmuri cluster with confidence ellipses.

Figure 8r: Final absolute locations (unbiased). The map shows the calibrated locations for the Murmuri cluster with confidence ellipses.

Figure 8s: Final absolute locations (unbiased). The map shows the calibrated locations for the Murmuri cluster with confidence ellipses.

Figure 8t: Final absolute locations (unbiased). The map shows the calibrated locations for the Murmuri cluster with confidence ellipses.

Figure 8u: Final absolute locations (unbiased). The map shows the calibrated locations for the Murmuri cluster with confidence ellipses.

Figure 8v: Final absolute locations (unbiased). The map shows the calibrated locations for the Murmuri cluster with confidence ellipses.

Figure 8w: Final absolute locations (unbiased). The map shows the calibrated locations for the Murmuri cluster with confidence ellipses.

Figure 8x: Final absolute locations (unbiased). The map shows the calibrated locations for the Murmuri cluster with confidence ellipses.

## 6 From clusters to regional catalogs

Our calibrated relocation analyses are restricted to areas with dimensions of  $\sim 100$  km and are ill-suited for clusters with large numbers ( $>200$ ) of events.

We are currently incorporating **Bayesloc** in order to expand the relocation across a much larger region with large numbers of earthquakes, whilst retaining a rigorous assessment of location error.

**Bayesloc** is a multiple-event relocation algorithm [Myers et al., 2007, JGI], that accepts probabilistic, a priori constraints on all of the model parameters, enabling it to integrate both trusted data sets, such as clusters calibrated with **mloc**, and poor quality data sets.

It uses a Markov Chain Monte Carlo method for solving large scale, non-linear stochastic inverse problems, which reduces the assumptions from linearized relocation techniques and also allows us to relocate all of the instrumentally-recorded earthquakes in Iran.

**Bayesloc** was already applied to  $>5,000$  events in Middle East [Myers et al., 2011, JGR] yielding mislocations of  $\sim 5$  km with respect to the available GT1 epicenters, but in this instance no local or regional calibration was used.